Analytica Chimica Acta 1147 (2021) 108–115

Contents lists available at ScienceDirect

Analytica Chimica Acta

journal homepage: www.elsevier.com/locate/aca

# Ultrasensitive electrochemical biosensor for attomolar level detection of let 7a based on toehold mediated strand displacement reaction circuits and molecular beacon mediated circular strand displacement polymerization

Zhang Zhang [a, b], Li Zhang [a], Youqiang Wang [c], Juan Yao [c], Ting Wang [a, d], Zhi Weng [a], Liu Yang [a], Guoming Xie [a, *]

[a] Key Laboratory of Laboratory Medical Diagnostics of Education, Department of Laboratory Medicine, Chongqing Medical University, Chongqing, PR China
[b] Department of Laboratory Medicine, The Affiliated Hospital of Southwest Medical University, Luzhou, PR China
[c] Department of Laboratory Medicine, The Affiliated Traditional Chinese Medicine Hospital of Southwest Medical University, Luzhou, PR China
[d] Department of Laboratory Medicine, Chongqing Fuling People's Hospital, Chongqing, PR China

## HIGHLIGHTS

- A multiple amplification strategy based on SDRCs and ICSDPR was designed.
- The SDRCs and ICSDPR process exhibited good selectivity and amplified the signal efficiently.
- The method exhibited high sensitivity with the LOD of 6.2 aM for miRNA let 7a.
- The proposed strategy achieved extensive prospect in complex matrix and real samples of cells.

## GRAPHICAL ABSTRACT

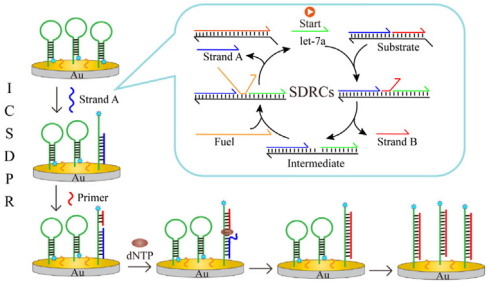


## ARTICLE INFO

*Article history:*
Received 23 August 2020
Received in revised form
26 November 2020
Accepted 27 December 2020
Available online 30 December 2020

*Keywords:*
Electrochemical biosensor
Non-coding RNA marker
Molecular beacons
Circular strand displacement circuits
Isothermal circular strand displacement polymerization reaction

## ABSTRACT

In this study, an ultrasensitive electrochemical miRNA biosensor based on toehold mediated strand displacement reaction circuits (SDRCs) and molecular beacon mediated isothermal circular strand displacement polymerization reaction (ICSDPR) has been proposed. During the SDRCs module, the cascade strand displacement reaction induces the recycling of the target let 7a and generation of a large amount of strand A (SA). The SA recognition opens the hairpin capture probe immobilized on the gold electrode, thus, varying the distance between the redox molecules and electrode surface. The primer mediated ICSDPR is observed to further generate a large amount of SA, thus, leading to a reduction in the signal. Considering these merits, the proposed method is observed to exhibit a log-linear linearity from 10 aM to 100 pM and ultrahigh sensitivity towards let 7a down to 6.2 aM, with a capability of distinguishing the let 7a family members, thereby, providing a new electrochemical route for early cancer screening.



* Corresponding author.
*E-mail addresses:* guomingxie@cqmu.edu.cn, 504524429@qq.com (G. Xie).

https://doi.org/10.1016/j.aca.2020.12.057
0003-2670/

## 1. Introduction

The function of RNA in the cell is to assist in the translation of the genetic information from DNA into protein. The major RNA species include messenger RNA, transfer RNA and ribosomal RNA [1–3]. Recently, the technological advances and improvements in the RNA analysis and detection have led to the discovery of new classes of small and large non-coding RNAs containing novel regulatory functions, such as microRNA (miRNA) [4,5], circular RNA [6,7], long non-coding RNA [8], small nucleolar RNA [9,10] and extracellular RNA [11,12]. miRNAs represent a class of stable endogenous single-stranded phylogenetically conserved RNA (20–24 nucleotides) and play a critical role for controlling the gene expression at the post-transcriptional level. Owing to this, miRNAs have been widely accepted as potential biomarkers for conducting clinical diagnosis and prognosis. Specifically, miRNAs function mainly post-transcriptionally by binding with the 3′ untranslated region of the target messenger RNA (mRNA), thus, inducing mRNA degradation or translational repression [13,14]. Over the past few years, different strategies have been developed for miRNA detection, relying mainly on real time quantitative reverse transcription PCR (RT-qPCR) [15,16], microarray [17,18] and sequencing [19,20]. Microarray hybridization and sequencing are high throughput methods and exhibit high efficiency in large scale screening, however, these processes are labor expensive and time consuming. RT-qPCR has been widely applied for RNA detection, however, the requirement of reverse transcription usually results in substantial sample loss and variation [21]. The challenges associated with miRNA detection include low abundance and high sequence homology of miRNA [22]. Therefore, novel detection approaches are vitally needed to overcome these challenges. The strand displacement reaction (SDR), first introduced by Yurke et al. is an enzyme-free molecular tool to exchange one type of nucleic acids strand with another [23]. Due to superior design, selectivity and operation flexibility as compared with other hybridization probes such as molecular beacons, SDR has found widespread use to generate basic building blocks in the field of DNA nanotechnology for designing the reconfigurable structures [24,25], logic gates [26,27], DNA machines [28,29], and biosensors [30,31]. Among these, toehold mediated strand displacement reaction cascades (SDRCs) with robust response to the temperature and salt conditions have gained extensive attention. SDRCs is a kind of cascade amplification strategy based on the principle of toehold exchange. It is a spontaneous phenomenon driven by entropy without enzymes. Due to its programmability and universality, the signal amplification technology based on SDRCs has been used to construct various biosensors. For instance, Yin et al. developed a biosensor for HIV related gene detection [32], In another study, Li et al. developed a biosensor for tumor cell detection [33]. However, this method is limited by its unsatisfactory sensitivity, thus, it cannot satisfy the sensitivity needed for miRNA detection.

In recent years, molecular beacons based isothermal circular strand displacement polymerization reaction (ICSDPR), as isothermal DNA amplification method, has been reported to improve the sensitivity and specificity of the biosensors [34,35]. In ICSDPR, the hybridization between the capture probe and DNA leads to the polymerization reaction in the presence of a primer. The released DNA subsequently opens another capture probe to initiate the polymerization reaction, thereby, resulting in the recycling of the target DNA and achievement of the signal amplification. Compared with other amplification techniques such as PCR, exonuclease-based methods [36,37], and rolling circle amplification [38,39], ICSDPR does not require cumbersome thermal cycling, specific recognition site and specially designed circular template. Thus, ISDPR can be conveniently employed to fabricate the DNA biosensors.

In this study, SDRCs and ICSDPR have been combined to develop a simple and ultrasensitive electrochemical biosensor for specific detection of let 7a, by successfully achieving target recycling mediated cascade amplification and primer mediated displacement cycle. The redox methylene blue (MB) tag represents the distance variation in the gold electrode surface and has been detected via the electrochemical square wave voltammetry (SWV) measurements. Overall, the proposed electrochemical biosensor exhibited optimal analytical performance towards let 7a detection, thereby, providing a rapid and convenient sensing platform for nucleic acid detection. One of the major advantages of our approach is that significant signal amplification can be achieved. Thus, the proposed method presents a simple and effective platform for nucleic acids screening in applications such as bioanalysis, clinical diagnosis and pathogen detection.

## 2. Experimental

### 2.1. Reagents

miRNAs and HPLC-purified DNA oligonucleotides were provided by Sangon Biotech (Shanghai, China). The sequences of the nucleic acids employed in the study are shown in Table S1. The oligonucleotides were dissolved in the TE buffer (pH 8.0, 10 mM Tris–HCl, 1 mM EDTA) and stored at −20 °C, followed by dilution in the hybridization buffer (50 mM Tris–HCl, pH 7.4 and 100 mM NaCl) prior to use. Polymerase Klenow fragment exo$^-$ and dNTPs were purchased from New England Biolabs (USA). The magnetic beads were obtained from Roche Life Science (Switzerland). miRNAs real-time PCR assay were carried out using the stem-loop method to obtain cDNA as well as the SYBR green quantify method. All other reagents were of analytical grade. 6-Mercapto-1-hexanol (MCH) and diethylpyrocarbonate (DEPC) were purchased from Sigma-Aldrich (St Louis, USA). The ultrapure water was obtained using the Millipore water purification system (>18 MΩ, Milli-Q, Millipore). To avoid miRNA degradation, the buffer solutions were treated with 0.1% DEPC. Total RNA was extracted from human breast adenocarcinoma 231 and Hs 578Bst breast cells via Trizol method.

### 2.2. Apparatus

The fluorescence measurements were carried out using a Cary Eclipse Fluorescence spectrophotometer (Agilent, USA) by employing an excitation wavelength of 485 nm and emission wavelength in the range 500–560 nm. Gel electrophoresis was performed by using an electrophoresis system (DYY-6C, LIUYI, China). The gel images of 12% native PAGE were captured using an imaging system (Bio-Rad Laboratories, USA). The concentration of the cell extracts was measured using UV–visible absorption spectroscopy (NANO-DROP1000 Spectrophotometer, Thermo, USA). The fluorescent images of the magnetic particles were obtained using fluorescence microscopy equipped with 20 objective (Olympus IX 71, Tokyo, Japan) and CoolSNAPcf charge coupled device (CCD) camera (Photometrics, Tucson, AZ) with Metamorph image analysis software (Molecular Devices, Sunnyvale, CA). For the analysis, the samples were extensively washed with PBS. The reverse transcription and miRNA real time PCR were performed in a CFX 96 real time detection system (Bio-Rad, USA). A CHI660D electrochemical workstation (Shanghai, China) was employed for the experiments. It contained a normal three-electrode system, including a Pt wire auxiliary electrode, an Ag/AgCl reference electrode and a 3 mm diameter gold disk electrode as the working electrode.

### 2.3. Preparation of DNA nanomachine

For preparing the SDRCs based DNA nanomachine, a 50 μL reaction mixture containing 200 nM each of substrates and fuel strand with different concentrations of the miRNAs target were incubated for 30 min at 25 °C for development as electrochemical biosensor.

### 2.4. Fabrication of electrochemical sensor surface

Biosensors were fabricated by employing the standard approaches. Briefly, the gold disk electrodes were prepared by polishing with 0.3 and 0.05 μm alumina slurry. It was followed by sonication in ultrapure water, ethanol and ultrapure water for 5 min each, respectively. Subsequently, the electrodes were cleaned in the piranha solution (1:3$H_2O_2$/$H_2SO_4$ by volume) for 10 min, followed by rinsing with distilled water. Further, 10 μL of 1 μM thiolated capture probe was dropped on the pretreated gold electrode surface, followed by incubation at 4 °C overnight. After washing with hybridization buffer, the electrode was immersed in 10 μL of 1 mM MCH for 1 h so as to obtain a well-aligned DNA monolayer occupying the left bare sites. 10 μL SDRCs products were further dropped on the electrode at room temperature for 1 h. After washing, 10 μL ICSDPR mixture consisting of 100 nM primer, 500 μM dNTPs and 5U klenow fragment (KF) was dropped on the electrode surface for 2 h at 37 °C. Subsequent to washing, SWV measurements were performed in the hybridization buffer in triplicate.

### 2.5. Magnetic particles characterization

10 μL streptavidin loaded magnetic particles was mixed with 10 μL of 1 μM biotin capture probe at room temperature for 30 min. Upon magnetic separation, the beads were collected and rinsed for three times. Then 10 μL SDRCs products were added and incubated for 1 h. After magnetic separation, 10 μL ICSDPR mixture consisting of 100 nM primer, 500 μM dNTPs and 5U KF were added for 2 h at 37 °C. Subsequent to magnetic separation and resuspend, the mixture were used for fluorescence imaging.

### 2.6. Cell culture and total RNA extraction

Human breast adenocarcinoma 231 and Hs 578Bst cells were cultured in Dulbecco's modified Eagle's medium (HyClone, USA) supplemented with 10% fetal bovine serum (Gibco Life Technologies, USA) and 100 U/mL streptomycin/penicillin at 37 °C in 5% $CO_2$. Total RNAs were extracted using TRIZOL method, followed by concentration measurement. The final stocks of total RNA with a concentration of 0.5 μg/μL were stored at 80 °C.

### 2.7. RT-PCR assay

miRNA was first reversibly transcribed to obtain cDNA using the stem-loop method. The RT-PCR reaction mixture included 10 μL 2*miRNA master mix, 0.5 μL of 10 μM forward and reverse primers, 1 μL cDNA and 8 μL DEPC-treated water. The qRT-PCR process was performed using the following conditions: 95 °C for 1 min, followed by 40 cycles at 95 °C with 5 s per cycle, 60 °C for 15 s and 72 °C for 15 s.

## 3. Results and discussion

### 3.1. Principle and design of the sensing system

The sensing mechanism associated with the let 7a target triggered cascade amplification strategy has been depicted in Scheme 1. The sensing system comprises of non-enzymatic let 7a recycling amplification and isothermal circular strand-displacement polymerization reaction. The detailed secondary structures have been predicted by NUPACK, as shown in Fig. S1. For non-enzymatic amplification of target recycling, the system uses three strands substrate composed of linker, strand A (SA) and strand B (SB). In the presence of let 7a, hybridization with the toehold region of the linker induced the displacement of SB. Subsequently, let 7a hybridized with the middle region of the linker. Further, both SA and let 7a were displaced by the fuel strand, and the released let 7a initiated the next reaction cycle. Thus, an ample amount of SA was generated for further electrochemical signal amplification.

A hairpin-structured probe, dually labeled with 5′ SH and 3′ MB, possessed a stem of 10 base pairs enclosing a loop of 19 unpaired nucleotides. The loop region was complementary to SA, whereas the 3′ terminal of the stem portion corresponded to the primer. The hairpin probe was first self-assembled on the gold electrode through Au–S binding, followed by MCH immobilization for keeping it straight. Thus, MB exhibited an efficient electrochemical activity owing to the closeness to the gold electrode surface. The hairpin probe hybridized to form duplex on interaction with SA, thus, leading the MB molecules away from the gold electrode surface. As a result, the distance variation associated with MB resulted in a decreased electrochemical current response. Further, the primer hybridized with the stem region of the probe at 3' end, thus, triggering the polymerization reaction in the presence of dNTPs/polymerase. This process of primer extension resulted in the displacement of SA, with the replaced SA subsequently binding with another hairpin probe to trigger the second polymerization cycle. Eventually, each SA was observed to undergo many cycles, which led to more MB molecules moving away from the electrode surface, thus, dramatically decreasing the electrochemical signal.

### 3.2. Characterization of biosensor

Cyclic voltammetry (CV) and electrochemical impedance spectroscopy (EIS) were employed to characterize the biosensor fabrication. The larger semicircle diameter in EIS plots represents the electrode-transfer resistance (Ret) of the modified electrode. As shown in Fig. 1A, the bare gold electrode demonstrated an obvious peak current in CV (curve a). On decoration with the hairpin shaped capture probe via Au–S bonding, the CV current response decreased, with the enlargement of the separation degree between the two peaks (curve b). The reason for the observed phenomenon is the electrostatic repulsion between the negatively charged deoxyribose-phosphate backbone of the capture probe and $[Fe(CN)_6]^{3-/4-}$. On adding MCH to remove the non-specifically adsorbed capture probe, a large decrease in the peak current as well as an enlarged peak-to-peak separation could be observed (curve c). Hybridizing with SA led to a further decrease in the redox current and enlargement of the peak separation (curve d), due to the insulating behavior of the duplexed DNA strands, thus, implying the hybridization between capture probe (CP) and SA. On incubating the electrode with the polymerase reaction mixture, the lowest redox peak was obtained (curve e) due to the production of a large amount of dsDNA owing to the polymerase reaction. The impedance data was further fitted using a Randles equivalent circuit based on ZSimpWin version 3.10. The equivalent electrical circuit consisted of an active electrolyte resistance (Rs) in series with a constant phase element (CPE), along with a faradaic reaction impedance (Ret) in parallel with Warburg impedance ($Z_W$). The observed changes in EIS (Fig. 1B) were in good agreement with the CV method, which further demonstrated that the electrochemical

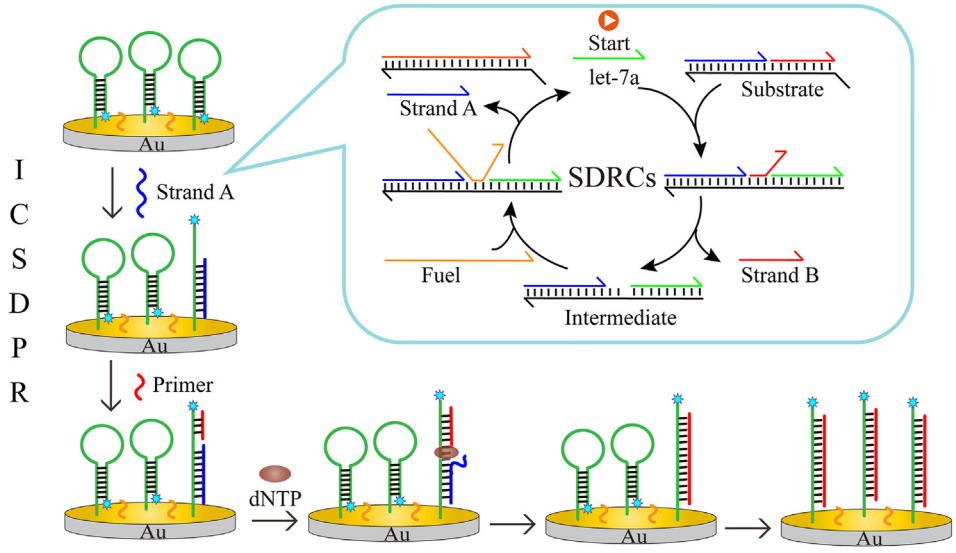


**Scheme 1.** Scheme illustration of let 7a electrochemical detection based on SDRCs and ICSDPR.

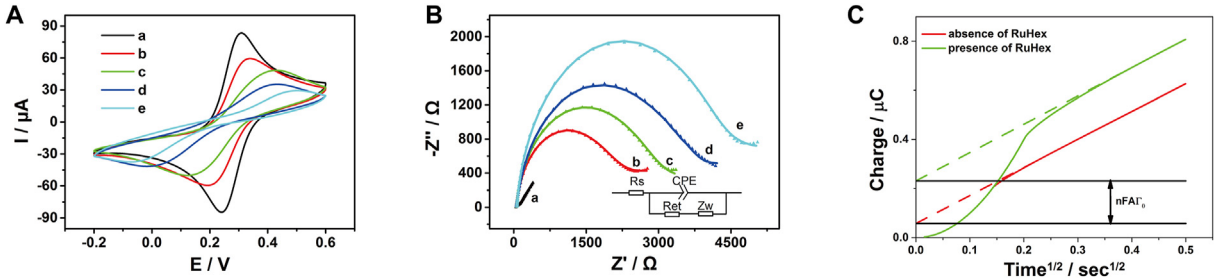


**Fig. 1.** CV (A) and EIS (B) characterization of the bare gold electrode (curve a), CP modified electrode (curve b), MCH immobilized electrode surface (curve c), CP modified electrode after hybridization with SA (curve d) and surface after ICSDPR (curve e). Inset shows the equivalent circuit used to model the impedance data. (C) Determination of coupled 39-mer CP density via chronocoulometry. Extrapolated y-intercepts shown by dotted lines indicate the surface excess charge for measurements with (green curve) and without (red curve) RuHex. (For interpretation of the references to colour in this figure legend, the reader is referred to the Web version of this article.)

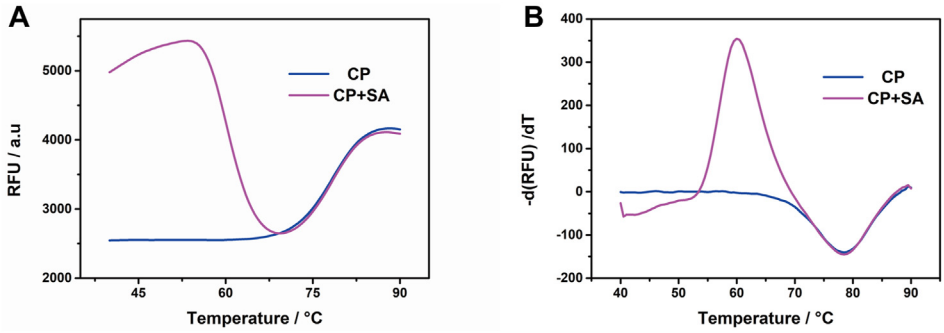


**Fig. 2.** Melting curves (A) and normalized derivative melting curves (B) of CP and CP/SA duplex.

biosensor was successfully fabricated.

Melting curve analyses were further carried out to characterize the hairpin capture probe. During melting analysis (Fig. 2A and B), the CP stem structure was destroyed on enhancing the temperature, thus, forming a single strand. It led to the separation between the quencher and fluorophore. For CP and SA duplex, the fluorescence intensity was noted to be high at low temperature due to the duplex leading away from the quencher and fluorophore. On enhancing the temperature, the duplex was observed to anneal and CP reformed the hairpin structure, thus, leading to a reduction in fluorescence. For temperature greater than 68 °C, the hairpin structure got destroyed and fluorescence was enhanced. The melting temperature for CP and CP/SA duplex was observed to be 61 and 79 °C, thus, demonstrating an optimal correlation with the Gibbs energy change (see Table S2). The observed results indicate the successful fabrication of CP and stability at low temperature, along with the successful hybridization between CP and SA.

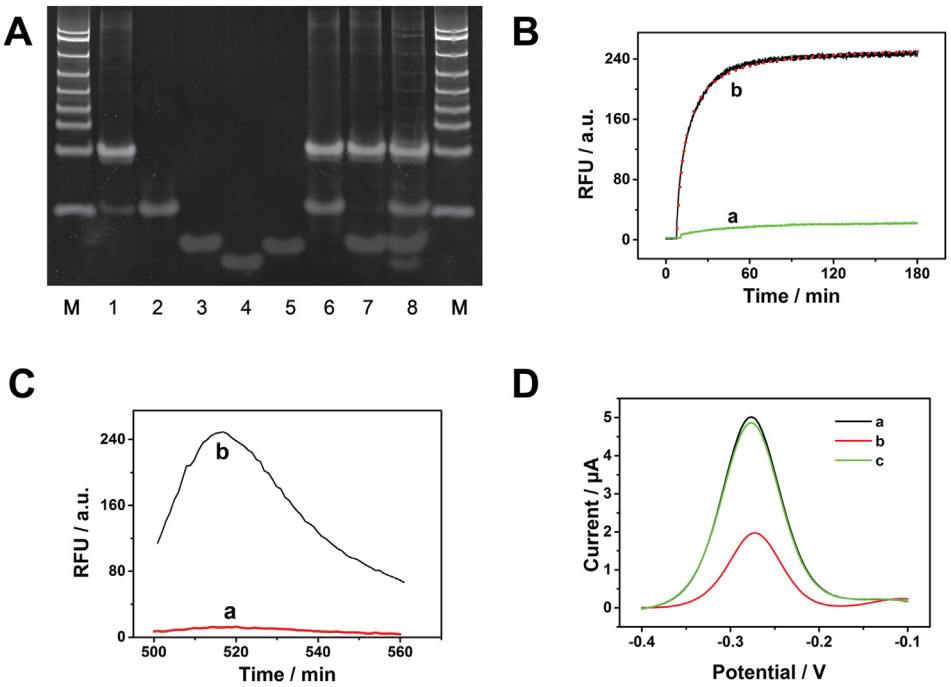


**Fig. 3.** (A) 12% native PAGE of the 500 nM substrate (lane 1), fuel strand (lane 2), let 7a (lane 3), SA (lane 4), SB (lane 5), substrate/fuel (lane 6), substrate/let 7a (lane 7) and substrate/fuel/let 7a (lane 8). (B) Kinetics and (C) fluorescence emission spectrum curves of SDRCs with and without the target let 7a, where the dotted line represents the simulated curve based on the second order reaction rules. (D) Feasibility investigation of the electrochemical biosensor: SWV response of (a) CP/MCH/electrode, (b) CP/MCH/electrode + let 7a and (c) negative control.

### 3.3. Feasibility of the electrochemical biosensor

The amplification of the SDRCs system was analyzed by using 12% polyacrylamide gel electrophoresis for validity. As shown in Fig. 3A, the substrate, fuel, let 7a, SA and SB exhibited distinctive bands (lane 1 to lane 5). The lanes 6 and 7 indicated that the fuel or let 7a cannot individually displace SA and SB from the substrate. On adding the substrate, let 7a and fuel, SDRCs led to the release of SA and SB, along with forming a new band (lane 8). The kinetics and fluorescence spectrum were further analyzed to demonstrate the SDRCs system. As shown in Fig. 3B, omitting let 7a did not result in any obvious signal (curve a) due to the quenching of FAM fluorescence by Dabcyl upon hybridization between SA and linker. In contrast, the fluorescence intensity was observed to gradually increase on adding 1 pM let 7a (curve b), thus, implying that SDRCs was successfully initiated. Fig. 3C shows the corresponding fluorescence emission spectrum at 180 min, demonstrating optimal accordance with the kinetic results. The SWV measurements were employed to analyze the changes in the electrochemical properties during the modification process. As exhibited in Fig. 3D, a strong MB signal was observed at −0.264 V after immobilization of MB labeled CP (curve a). On further incubating the modified Au electrode with the SDRCs product and initial ICSDPR, the MB response was noted to be significantly suppressed (curve b), whereas a slight change was observed for the negative control (curve c). The observed results indicated the successful fabrication of the electrochemical biosensor, along with a readily measured current variation in the presence of let 7a. To further demonstrate the feasibility of ICSDPR on the electrode surface, streptavidin loaded magnetic particles were used for monitoring the process. The images of the magnetic particles in white light and corresponding fluorescence after ICSDPR are shown in Fig. 4A and B. The observed findings reconfirmed the successful fabrication of the biosensor.

### 3.4. Optimization of experimental conditions

Various vital experimental parameters including capture probe concentration, immobilization time, primer length and polymerization duration were optimized to achieve the effective performance of the electrochemical biosensor. In case a reaction condition was optimized, the other parameters were maintained at the optimized conditions or the longest reaction durations and highest concentrations.

The probe density (Γ) is an important parameter in biosensing as it affects the probe's orientation and uniformity of the sensing layer. Γ value should be rational as too few probes may influence the sensitivity for hybridization, whereas a high density may decrease the hybridization efficiency due to electrostatic repulsion. Therefore, for this purpose, CP concentration and incubation duration were evaluated. As shown in Fig. S2A, △I (change in SWV current, which represents the peak current variation for the polymerase reaction mixture with and without SA) reached a maximum at a concentration of 0.6 μM. Further increase in the CP concentration resulted in a slight decrease in the value of the signal change. The dependence of △I on the self-assembly duration was studied from 2 to 12 h (Fig. S2B). It was observed that △I increased gradually with time and stabilized after 8 h. Thus, 8 h duration was selected as the optimal deposition time for the developed electrochemical biosensor. Further, Γ was verified to be $7.85*10^{11}$ molecules/$cm^2$ (Fig. 1C). The primer length is a vital factor for ICSDPR, and the effect of the primer length has been presented in Fig. S2C, where the red pillar represents the current variation induced by ICSDPR. As expected, △I was observed to reach a maximum length of 8 nt. The observed phenomenon was attributed to the fact that the short primer may decrease the hybridization between primer and CP, whereas the long primer may deteriorate the unspecific hybridization. On enhancing the polymerization time (Fig. S2D), the current change was noted to increase and tended to a steady value

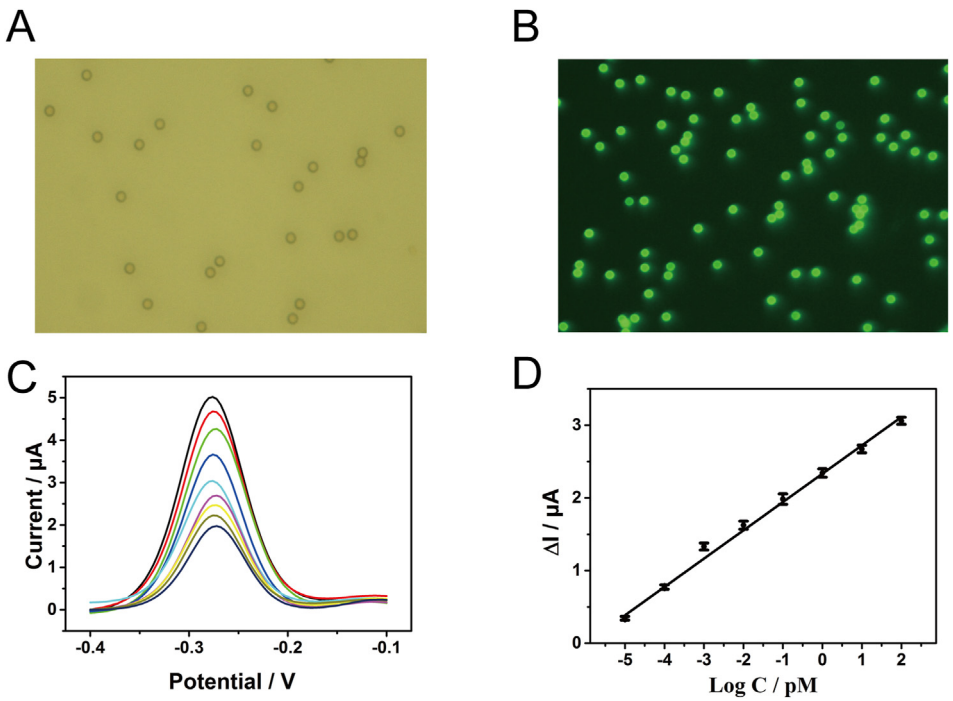


**Fig. 4.** Images of the magnetic particles in white light (A) and fluorescent images after (B) SDRCs and ICSDPR. (C) SWV response of the electrochemical biosensor as a function of the concentration of the complementary DNA (from top to bottom: 0, 10 aM, 100 aM, 1 fM, 10 fM, 100 fM, 1 pM, 10 pM and 100 pM). (D) Linear relationship between the current change and let 7a concentration. The error bars represent the standard deviations of the measured values (n = 3).

at 120 min. Further enhancing the time did not improve the response, thus, 120 min duration was chosen as the optimal condition.

### 3.5. Sensitivity of the designed approach

The sensitivity of the fabricated biosensor was evaluated using concentrations series of let 7a under optimal conditions. As shown in Fig. 4C, the signal decreased on increasing the target concentration. As a result, a higher extent of CP opened, thus, pushing MB away from the electrode surface. The calibration curve demonstrated a linear relationship between the peak current change and logarithmic values of let 7a in the range from 10 aM to 100 pM. The corresponding regression equations can be expressed as: $\triangle I = 0.39*\text{Log C (pM)} + 2.33$, with the value of the coefficient of determination ($R^2$) as 0.98 (Fig. 4D). The detection limit for the proposed biosensor was estimated at 6.2 aM at signal to noise equals three rules. Overall, the proposed biosensor demonstrated optimal performance in terms of analytical range and detection limit, in accordance with the previous study (See Table S4).

### 3.6. Selectivity and real sample analysis

The small size and sequence similarity of the let 7 families significantly complicate the miRNA detection, and a sequence mismatch can correspondingly produce a false positive signal. The specificity of the proposed miRNA biosensor in this study was investigated by detecting the various sequences contained in the let 7 families. As shown in Fig. 5A, the presence of the non-target substances resulted in an insignificant change in the current response. The high specificity of the biosensor might have contributed to the strict sequence requirements for the circular strand displacement reaction. Further, the extracted RNAs from 231 and Hs 578Bst cell lines were analyzed using the proposed method, followed by comparison with the standard RT-PCR. As shown in Fig. 5B and C, the real-time fluorescence intensity enhanced in a sigmoidal fashion on changing the concentration of let 7a. The threshold cycle (Ct) value exhibited a linear correlation with the logarithm of the concentration of let 7a in the range from 100 aM to 1 pM. The corresponding melting curves are also shown in Fig. S3, indicated the specificity of RT-PCR. The amount of let 7a in the two cell lines was observed at different levels, thus, the proposed method exhibited a good agreement with RT-PCR (Fig. 5D). In addition, different amounts of let 7a with known concentrations were used to further analyze the accuracy of the proposed method. The recovery rate was observed in the range from 97.8 to 102.9% (Table S3), which clearly indicated that the developed method has a significant promise for practical applications with respect to accurate and reliable miRNA detection.

## 4. Conclusion

In conclusion, the fabrication of a simple, sensitive and specific electrochemical let 7a biosensor has been demonstrated by the combination of isothermal SDRCs and ICSDPR. The merits of SDR enable the high sequence specificity, and the two cascades circuit enables high sensitivity. SDRCs could be autonomously operated together with the let 7a target recycling, leading to the generation of a large amount of SA to execute ICSDPR. The successive ICSDPR correspondingly induced the conformational change in the stem-loop structure, thus, leading to the electrochemical signal change. Thus, the current modular and cascade operation including SDRCs and successive ICSDPR process concertedly endow the detection of let 7a with high sensitivity and confidence level. As a result, a low detection limit of about 6.2 aM with an excellent selectivity towards the target miRNA could be achieved. Overall, the proposed approach represents a promising tool for miRNAs research as well as bimolecular and early diagnosis of diseases due to the unique characteristics of low cost, flexibility in sequence design and fabrication simplicity.

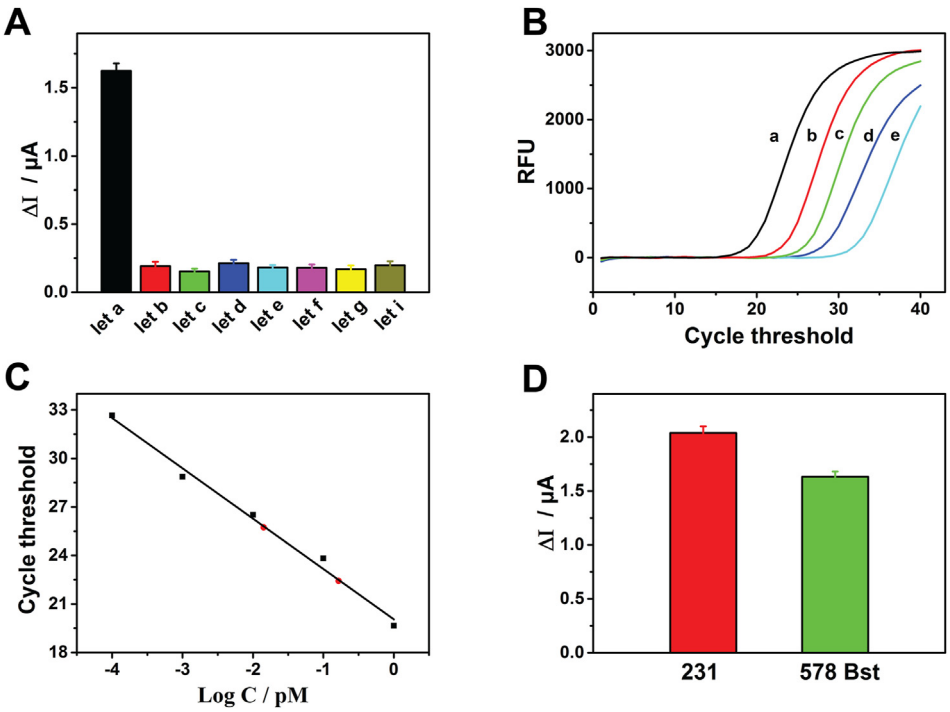


**Fig. 5.** (A) SWV current changes corresponding to let 7a, let 7b, let 7 c, let 7 d, let 7 e, let 7 f, let 7 g and let 7 i. (B) The RT-PCR results for the different concentrations let 7a target (from curve a to e: 1 pM, 100 fM, 10 fM, 1 fM and 100 aM). (C) The linear relationship between Ct value and let 7a concentration. Red dots demonstrate the findings from miRNA extracted from 231 and Hs 578Bst cell lines. (D) SWV current changes corresponding to the extracted miRNA from 231 and Hs 578Bst cell lines. (For interpretation of the references to colour in this figure legend, the reader is referred to the Web version of this article.)

## CRediT authorship contribution statement

**Zhang Zhang:** Conceptualization, Methodology, Writing - original draft. **Li Zhang:** Conceptualization, Data curation. **Youqiang Wang:** Writing - review & editing. **Juan Yao:** Conceptualization, Data curation. **Ting Wang:** Visualization, Investigation. **Zhi Weng:** Data curation. **Liu Yang:** Writing - review & editing. **Guoming Xie:** Writing - review & editing, Supervision, Funding acquisition.

## Declaration of competing interest

The authors declare that they have no known competing financial interests or personal relationships that could have appeared to influence the work reported in this paper.

## Acknowledgements

This research was supported by the National Natural Science Foundation of China (Grant No.81672112, 81802110 and 81902169) and Top Talent Project of Chongqing Medical University (BJRC 201909).

## Appendix A. Supplementary data

Supplementary data to this article can be found online at https://doi.org/10.1016/j.aca.2020.12.057.

## References

[1] I.A. Roundtree, C. He, RNA epigenetics—chemical messages for post-transcriptional gene regulation, Curr. Opin. Chem. Biol. 30 (2016) 46–51.
[2] P.G. Martini, L.T. Guey, A new era for rare genetic diseases: messenger RNA therapy, Hum. Gene Ther. 30 (2019) 1180–1189.
[3] T.M. Lowe, P.P. Chan, tRNAscan-SE On-line: integrating search and context for analysis of transfer RNA genes, Nucleic Acids Res. 44 (2016) 54–57.
[4] F.J. Ruiz-Ojeda, J. Plaza-Diaz, A. Gil, RNA Analyses, Principles of Nutrigenetics and Nutrigenomics, Elsevier, 2020, pp. 41–48.
[5] A. Kozomara, M. Birgaoanu, S. Griffiths-Jones, miRBase: from microRNA sequences to function, Nucleic Acids Res. 47 (2019) 155–162.
[6] J.N. Vo, M. Cieslik, Y. Zhang, S. Shukla, L. Xiao, Y. Zhang, Y.-M. Wu, S.M. Dhanasekaran, C.G. Engelke, X. Cao, The landscape of circular RNA in cancer, Cell 176 (2019) 869–881.
[7] J. Salzman, R.E. Chen, M.N. Olsen, P.L. Wang, P.O. Brown, Cell-type specific features of circular RNA expression, PLoS Genet. 9 (2013) 1003777–1003791.
[8] J.J. Quinn, H.Y. Chang, Unique features of long non-coding RNA biogenesis and function, Nat. Rev. Genet. 17 (2016) 47–62.
[9] M. McMahon, A. Contreras, M. Holm, T. Uechi, C.M. Forester, X. Pang, C. Jackson, M.E. Calvert, B. Chen, D.A. Quigley, A single H/ACA small nucleolar RNA mediates tumor suppression downstream of oncogenic RAS, Elife 8 (2019) 48847–48864.
[10] J. Cavaillé, K. Buiting, M. Kiefmann, M. Lalande, C.I. Brannan, B. Horsthemke, J.-P. Bachellerie, J. Brosius, A. Hüttenhofer, Identification of brain-specific and imprinted small nucleolar RNA genes exhibiting an unusual genomic organization, Proc. Natl. Acad. Sci. Unit. States Am. 97 (2000) 14311–14316.
[11] K.M. Danielson, R. Rubio, F. Abderazzaq, S. Das, Y.E. Wang, High throughput sequencing of extracellular RNA from human plasma, PloS One 12 (2017) 164644–164661.
[12] J. Rozowsky, R.R. Kitchen, J.J. Park, T.R. Galeev, J. Diao, J. Warrell, W. Thistlethwaite, S.L. Subramanian, A. Milosavljevic, M. Gerstein, exceRpt: a comprehensive analytic platform for extracellular RNA profiling, Cell Syst 8 (2019) 352–357.
[13] J. O'Brien, H. Hayder, Y. Zayed, C. Peng, Overview of microRNA biogenesis, mechanisms of actions, and circulation, Front. Endocrinol. 9 (2018) 402.
[14] L.F. Gebert, I.J. MacRae, Regulation of microRNA function in animals, Nat. Rev. Mol. Cell Biol. 20 (2019) 21–37.
[15] S. Andoorfar, S.A.H. Tafreshi, Z. Rezvani, Assessment of the expression level of miRNA molecules using a semi-quantitative RT-PCR approach, Mol. Biol. Rep. 46 (2019) 5057–5062.
[16] P. Androvic, N. Romanyuk, L. Urdzikova-Machova, E. Rohlova, M. Kubista, L. Valihrach, Two-tailed RT-qPCR panel for quality control of circulating microRNA studies, Sci. Rep. 9 (2019) 1–9.
[17] S. Roy, J.H. Soh, J.Y. Ying, A microarray platform for detecting disease-specific circulating miRNA in human serum, Biosens. Bioelectron. 75 (2016) 238–246.
[18] B. Liu, H. Yang, L. Taher, A. Denz, R. Grützmann, C. Pilarsky, G.F. Weber, Identification of prognostic biomarkers by combined mRNA and miRNA expression microarray analysis in pancreatic cancer, Transl, Oncol. 11 (2018) 700–714.
[19] M. Chu, S. Wu, W. Wang, L. Mao, Y. Yu, L. Jiang, W. Yuan, M. Zhang, L. Sang,

Q. Huang, miRNA sequencing reveals miRNA-4508 from peripheral blood lymphocytes as potential diagnostic biomarker for silica-related pulmonary fibrosis: a multistage study, Respirology 25 (2020) 511–517.
[20] B. Reichholf, V.A. Herzog, N. Fasching, R.A. Manzenreither, I. Sowemimo, S.L. Ameres, Time-resolved small RNA sequencing unravels the molecular principles of microRNA homeostasis, Mol. Cell 75 (2019) 756–768.
[21] A. Git, H. Dvinge, M. Salmon-Divon, M. Osborne, C. Kutter, J. Hadfield, P. Bertone, C. Caldas, Systematic comparison of microarray profiling, real-time PCR, and next-generation sequencing technologies for measuring differential microRNA expression, RNA 16 (2010) 991–1006.
[22] P. Gillespie, S. Ladame, D. O'Hare, Molecular methods in electrochemical microRNA detection, Analyst 144 (2019) 114–129.
[23] B. Yurke, A.J. Turberfield, A.P. Mills, F.C. Simmel, J.L. Neumann, A DNA-fuelled molecular machine made of DNA, Nature 406 (2000) 605–608.
[24] D. Han, S. Pal, Y. Liu, H. Yan, Folding and cutting DNA into reconfigurable topological nanostructures, Nat. Nanotechnol. 5 (2010) 712–717.
[25] Y. Zhang, V. Pan, X. Li, X. Yang, H. Li, P. Wang, Y. Ke, Dynamic DNA structures, Small 15 (2019) 1900228.
[26] H. Su, J. Xu, Q. Wang, F. Wang, X. Zhou, High-efficiency and integrable DNA arithmetic and logic system based on strand displacement synthesis, Nat. Commun. 10 (2019) 1–8.
[27] F.C. Simmel, B. Yurke, H.R. Singh, Principles and applications of nucleic acid strand displacement reactions, Chem. Rev. 119 (2019) 6326–6369.
[28] R. Zhang, J. Zhang, X. Qu, S. Li, Y. Zhao, S. Liu, Y. Wang, J. Huang, J. Yu, Efficient strand displacement amplification via stepwise movement of a bipedal DNA walker on an electrode surface for ultrasensitive detection of antibiotics, Analyst 145 (2020) 2975–2981.
[29] J. Hahn, W.M. Shih, Thermal cycling of DNA devices via associative strand displacement, Nucleic Acids Res. 47 (2019) 10968–10975.
[30] Z. Zhang, J. long Li, J. Yao, T. Wang, D. Yin, Z. Chen, G. Xie, Energy driven cascade recognition for selective detection of nucleic acids with high discrimination factor at room temperature, Biosens. Bioelectron. 79 (2016) 488–494.
[31] W. Tang, W. Zhong, Y. Tan, G.A. Wang, F. Li, Y. Liu, DNA strand displacement reaction: a powerful tool for discriminating single nucleotide variants, Top. Curr. Chem. 378 (2020) 1–30.
[32] D. Yin, Y. Tao, L. Tang, W. Li, Z. Zhang, J. Li, G. Xie, Cascade toehold-mediated strand displacement along with non-enzymatic target recycling amplification for the electrochemical determination of the HIV-1 related gene, Microchim. Acta. 184 (2017) 3721–3728.
[33] Y. Li, H. Chen, Y. Dai, T. Chen, Y. Cao, J. Zhang, Cellular interface supported toehold strand displacement cascade for amplified dual-electrochemical signal and its application for tumor cell analysis, Anal. Chim. Acta 1064 (2019) 25–32.
[34] Z. Yang, S. Zhang, H. Zhao, H. Niu, Z.-S. Wu, H.-T. Chang, Branched DNA junction-enhanced isothermal circular strand displacement polymerization for intracellular imaging of microRNAs, Anal. Chem. 90 (2018) 13891–13899.
[35] A.M. Solovjev, S.A. Kurzeev, I.Y. Sakharov, Chemiluminescent Microplate-Based Assay of DNA Based on Isothermal Circular Strand-Displacement Polymerization Reaction, ICSDPR, Talanta, 2020, p. 120895.
[36] M. Wang, Z. Fu, B. Li, Y. Zhou, H. Yin, S. Ai, One-step, ultrasensitive, and electrochemical assay of microRNAs based on T7 exonuclease assisted cyclic enzymatic amplification, Anal. Chem. 86 (2014) 5606–5610.
[37] C. Jiang, C. Yan, J. Jiang, R. Yu, Colorimetric assay for T4 polynucleotide kinase activity based on the horseradish peroxidase-mimicking DNAzyme combined with λ exonuclease cleavage, Anal. Chim. Acta 766 (2013) 88–93.
[38] N. Luo, Q. Xia, L. Zhang, Y. Zhang, L. Huang, Y. Zhang, J. Zhao, S. Ding, W. Cheng, One-step discrimination of BCR/ABLp210 transcript isoforms directly from RNA extraction with fusion-triggered rolling circle amplification, Anal. Chim. Acta 1067 (2019) 129–136.
[39] M.M. Ali, F. Li, Z. Zhang, K. Zhang, D.-K. Kang, J.A. Ankrum, X.C. Le, W. Zhao, Rolling circle amplification: a versatile tool for chemical biology, materials science and medicine, Chem. Soc. Rev. 43 (2014) 3324–3341.